MR Imaging of the Internal Auditory Canal and Inner Ear at 3T: Comparison between 3D Driven Equilibrium and 3D Balanced Fast Field Echo Sequences

Jun Soo Byun, MD[1,2]
Hyung-Jin Kim, MD[1]
Yoo Jeong Yim, MD[1]
Sung Tae Kim, MD[1]
Pyoung Jeon, MD[1]
Keon Ha Kim, MD[1]
Sam Soo Kim, MD[3]
Yong Hwan Jeon, MD[3]
Jiwon Lee, MD[3]

Index terms:
Temporal bone, MR
Cisternography, MR
Magnetic resonance (MR), pulse sequences
Magnetic resonance (MR), high-field-strength imaging

DOI:10.3348/kjr.2008.9.3.212

Korean J Radiol 2008;9:212-218
Received October 26, 2007; accepted after revision February 5, 2008.

[1]Department of Radiology and Center for Imaging Science, Samsung Medical Center, Sungkyunkwan University School of Medicine, Seoul 135-710, Korea; [2]Department of Radiology, Chung-Ang University Yongsan Hospital, Seoul 140-757, Korea; [3]Department of Radiology, Kangwon National University College of Medicine, Chuncheon 200-947, Korea

Address reprint requests to:
Hyung-Jin Kim, MD, Department of Radiology and Center for Imaging Science, Samsung Medical Center, Sungkyunkwan University School of Medicine, 50 Irwon-dong, Gangnam-gu, Seoul 135-710, Korea.
Tel. (822) 3410-6451
Fax. (822) 3410-2559
e-mail: hyungkim@skku.edu

Abbreviations:
bFFE = balanced fast field echo
CISS = constructive interference in the steady state
CNRs = contrast-to-noise ratios
CPA = cerebellopontine angle
CSF = cerebrospinal fluid
DRIVE = driven equilibrium
FASE = fast asymmetrical spin-echo
FGRE = fast gradient-echo
FRFSE = fast recovery fast spin-echo
FSE = fast spin-echo
IAC = internal auditory canal
NSA = number of signal average
SAR = specific absorption rate
SNR = signal-to-noise ratio

Objective: To compare the use of 3D driven equilibrium (DRIVE) imaging with 3D balanced fast field echo (bFFE) imaging in the assessment of the anatomic structures of the internal auditory canal (IAC) and inner ear at 3 Tesla (T).

Materials and Methods: Thirty ears of 15 subjects (7 men and 8 women; age range, 22−71 years; average age, 50 years) without evidence of ear problems were examined on a whole-body 3T MR scanner with both 3D DRIVE and 3D bFFE sequences by using an 8-channel sensitivity encoding (SENSE) head coil. Two neuroradiologists reviewed both MR images with particular attention to the visibility of the anatomic structures, including four branches of the cranial nerves within the IAC, anatomic structures of the cochlea, vestibule, and three semicircular canals.

Results: Although both techniques provided images of relatively good quality, the 3D DRIVE sequence was somewhat superior to the 3D bFFE sequence. The discrepancies were more prominent for the basal turn of the cochlea, vestibule, and all semicircular canals, and were thought to be attributed to the presence of greater magnetic susceptibility artifacts inherent to gradient-echo techniques such as bFFE.

Conclusion: Because of higher image quality and less susceptibility artifacts, we highly recommend the employment of 3D DRIVE imaging as the MR imaging choice for the IAC and inner ear.

Through the display of the fine anatomic structures of the internal auditory canal (IAC) and inner ear, high-resolution MR sequences using three-dimensional (3D) heavily T2-weighted fast imaging techniques have demonstrated an important role for the evaluation of various diseases of the temporal bone. Basically, two techniques denoted by various names are most widely used to provide high spatial resolution MR imaging of the temporal bone with a consistent cisternographic effect: 3D fast spin-echo (FSE) and 3D fast gradient-echo (FGRE) techniques (1−13).

Driven equilibrium (DRIVE), a synonym for fast recovery fast spin-echo (FRFSE), is an FSE sequence that uses a set of additional −90° recovery pulses applied at the end of the echo train to accelerate relaxation and reversion of the remaining transverse magnetization back to the longitudinal axis (5, 9, 12−14). Balanced fast field-echo (bFFE) is an FGRE sequence that utilizes a balanced gradient waveform for all gradient directions to provide a very high signal for tissues with a high T2/T1 ratio (8, 10, 13). There have been several studies that have compared the image quality of various 3D FSE and 3D FGRE sequences to demonstrate the anatomic structures of the IAC and inner ear (5, 6, 10, 12, 13); however, to the best of our knowledge, there

has been no study comparing the use of 3D DRIVE and 3D bFFE sequences at 3 Tesla (T). The purpose of this study was to compare 3D DRIVE and 3D bFFE sequences in the assessment of the anatomic structures of the IAC and inner ear with 3T MR.

MATERIALS AND METHODS

Thirty ears of 15 patients who were referred to our department to obtain brain MR imaging for various reasons were included in this study. All patients had no past medical history or clinical signs and symptoms related to ear diseases, and no patient had a significant abnormality as determined from the brain MR images. There were seven men and eight women in study, ranging in age from 22 years to 71 years, with a mean age of 50 years. The institutional review board approved this study and informed consent was obtained from each patient.

All MR examinations were performed on a whole-body 3T unit (Intera Achieva; Philips, Best, the Netherlands) by using an 8-channel sensitivity-encoding (SENSE) head coil. The maximum gradient amplitude and slew rate were 40 mT/m and 200 mT/m/ms, respectively. After completion of routine unenhanced MR imaging of the brain, a total of 60 sections of 0.6-mm thickness were obtained through the region of the cerebellopontine angle (CPA) by using both 3D DRIVE and 3D bFFE sequences. The imaging parameters for 3D DRIVE were 2000 ms/200 ms/1 (repetition time [TR] / echo time [TE] / number of signal average [NSA]), 90° flip angle, 336 × 335 matrix, 20-cm field of view, ± 23 kHz bandwidth, and 40 echo train length, with an acquisition time of 5 minutes 26 seconds. The imaging parameters used for 3D bFFE were 5.6 ms/2.3 ms/5 (TR/TE/NSA), 45° flip angle, 336 × 335 matrix, 20-cm field of view, and ± 36.5 kHz bandwidth that required an acquisition time of 3 minutes 59 seconds. Both MR sequences were performed in the axial plane with a SENSE factor of 2 without the use of contrast material. The specific absorption rate (SAR) limitation was set at 3.2 W/kg.

Two neuroradiologists reviewed both MR sequences and a final decision was made by consensus. During image interpretation, particular attention was paid on the visibility of the four branches of the cranial nerves within the IAC (the facial nerve, cochlear nerve, and superior and inferior vestibular nerves), the three turns of the cochlea (basal, middle, and apical), the modiolus and scalar septum of the cochlea, the vestibule, and three semicircular canals (superior, lateral, and posterior). Due to the inherent property of SENSE that can cause an inhomogeneous noise level among the slices and induce artificial suppression of background noise (13, 15), direct and constant measurement of background noise was mostly impossible, thus leading to the inability to obtain directly contrast-to-noise ratios (CNRs) from the acquired MR images. Accordingly, instead of measuring the CNRs of the cranial nerves within the IAC, we simply categorized the visibility of the cranial nerves within the IAC as good or bad based on visual inspection. Likewise, we visually graded the quality of the two MR sequences with respect to each anatomic structure

Table 1. Comparison of 3D DRIVE and 3D bFFE Sequences for Evaluation of Cranial Nerves within Internal Auditory Canal

Anatomic Structure	No. of Ears (%)		*P*
	3D DRIVE	3D FFE	
Facial nerve			0.793
Good	30/30 (100%)	28/30 (93.3%)	
Bad	0/30 (0%)	2/30 (6.7%)	
Cochlear nerve			0.691
Good	30/30 (100%)	27/30 (90%)	
Bad	0/30 (0%)	3/30 (10%)	
Superior vestibular nerve			0.793
Good	30/30 (100%)	28/30 (93.3%)	
Bad	0/30 (0%)	2/30 (6.7%)	
Inferior vestibular nerve			0.793
Good	30/30 (100%)	28/30 (93.3%)	
Bad	0/30 (0%)	2/30 (6.7%)	

Note.—DRIVE = driven equilibrium, bFFE = balanced fast field echo

Table 2. Comparison of 3D DRIVE and 3D bFFE Sequences for Evaluation of Anatomic Structures of Cochlea

Anatomic Structure	No. of Ears (%)		*P*
	3D DRIVE	3D FFE	
Apical turn			0.691
Good	30/30 (100%)	27/30 (90%)	
Bad	0/30 (0%)	3/30 (10%)	
Middle turn			1
Good	30/30 (100%)	30/30 (100%)	
Bad	0/30 (0%)	0/30 (0%)	
Basal turn			
(mean diameter, mm)			0.0002
on uppermost section	4.47 ± 1.22	3.99 ± 1.16	
on lowermost section	6.37 ± 1.17	5.38 ± 1.20	
Modiolus			0.896
Good	30/30 (100%)	29/30 (96.7%)	
Bad	0/30 (0%)	1/30 (3.3%)	
Scalar septum			0.0588
Good	20/30 (66.7%)	10/30 (33.3%)	
Fair	8/30 (26.7%)	20/30 (66.7%)	
Poor	2/30 (6.6%)	0/30 (0%)	

Note.—DRIVE = driven equilibrium, bFFE = balanced fast field echo

in the inner ear. As for the apical and middle turns and the modiolus of the cochlea, visibility was graded on a good-or-bad basis. In addition, we measured and compared the diameter at each slice in both MR sequences for the basal turn of the cochlea. As for the scalar septum of the cochlea, we visually graded the image quality as good, fair, and poor, where 'good' was defined as complete visualization, 'fair' as incomplete visualization with only minor defects, and 'poor' as incomplete visualization with major defects. We also graded the image quality for the vestibule and the three semicircular canals visually as good, fair, and poor, where 'good' was defined as complete visualization, 'fair' as visualization $\geq$ two-thirds of the anatomic structure concerned, and 'poor' as visualization < two-thirds of the anatomic structure concerned.

Statistical analysis was performed using the chi square test for the four branches of the cranial nerves within the IAC, the apical and middle turns of the cochlea, and the modiolus and scalar septum of the cochlea, and the paired *t* test was used for the cochlear basal turn. A *p* value of less than 0.05 was considered as statistically significant. As for the vestibule and three semicircular canals, we simply calculated percentages of each grade, because the data were inadequate for statistical analysis.

RESULTS

Both 3D DRIVE and 3D bFFE sequences using an 8-channel SENSE head coil with a SENSE factor of 2 satisfied the SAR limitation at 3T. The mean SARs of 3D DRIVE and 3D bFFE were 0.9 W/kg and 2.3 W/kg, respectively.

Visualization of the cranial nerves within the IAC and the anatomic structures in the inner ear as seen on 3D DRIVE and 3D bFFE is summarized in Tables 1–3. In both sequences, there was no case that showed significant

Table 3. Comparison of 3D DRIVE and 3D bFFE Sequences for Evaluation of Vestibule and Semicircular Canals

Anatomic Structure	No. of Ears (%)	
	3D DRIVE	3D FFE
Vestibule		
Good	29/30 (96.7%)	0/30 (0%)
Fair	1/30 (3.3%)	28/30 (93.3%)
Poor	0/30 (0%)	2/30 (6.7%)
Lateral SCC		
Good	30/30 (100%)	4/30 (13.3%)
Fair	0/30 (0%)	14/30 (46.7%)
Poor	0/30 (0%)	12/30 (40.0%)
Superior SCC		
Good	30/30 (100%)	5/30 (16.7%)
Fair	0/30 (0%)	17/30 (56.7%)
Poor	0/30 (0%)	8/30 (26.7%)
Posterior SCC		
Good	30/30 (100%)	3/30 (10%)
Fair	0/30 (0%)	21/30 (70%)
Poor	0/30 (0%)	6/30 (20%)

Note.—DRIVE = driven equilibrium, bFFE = balanced fast field echo, SCC = semicircular canal

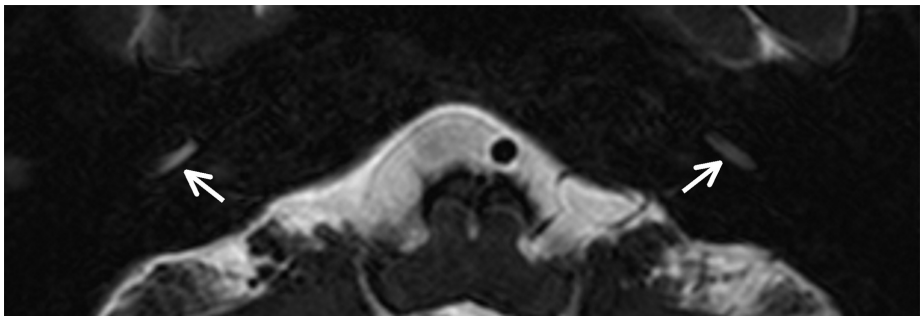

A

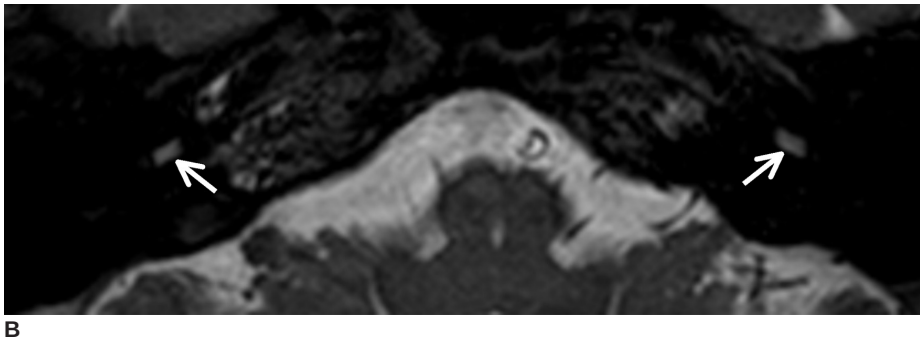

B

Fig. 1. Comparison of 3D driven equilibriumand 3D balanced fast field echo sequences for visualization of basal turn of cochlea. Diameter of basal turn of cochlea on both sides (arrows) is greater on 3D driven equilibrium image (**A**) than on 3D balanced fast field echo image (**B**).

cerebrospinal fluid (CSF) pulsation artifacts to hamper the evaluation of the cranial nerves at the CPA cistern and IAC. Although the statistical difference was not significant, a small degree of supremacy was noted with the use of 3D DRIVE over 3D bFFE for visualizing the four cranial nerve branches, the apical and middle turns of the cochlea, and the cochlear modiolus (Tables 1, 2). The basal turn of the cochlea was demonstrated better (statistically) on 3D DRIVE images than on 3D bFFE images ($p = 0.0002$, paired t-test) (Fig. 1). Although the scalar septum of the cochlea was also visualized somewhat better with the use of the 3D DRIVE sequence, significant statistical differences were not noted between the two sequences ($p = 0.0588$, chi square test) (Table 2). Although the image quality of 3D DRIVE for visualizing the vestibule and all of the three semicircular canals was apparently better than that of 3D bFFE, this was not demonstrated statistically (Table 3, Figs. 2, 3).

DISCUSSION

Various T2-weighted volume 3D fast MR imaging sequences, such as constructive interference in the steady-state (CISS), segment interleaved motion compensated acquisition in the steady state (SIMCAST), fast imaging employing steady-state acquisition (FIESTA), steady-state free precession (SSFP), true free induction with steady precession (trueFISP), bFFE, fast asymmetrical spin-echo (FASE), FRFSE, and DRIVE are commercially available for use in different MR units to display the cisternographic effect in the inner ear, IAC, and CPA. Basically, the two techniques most widely used are the 3D FSE and 3D FGRE techniques (1–13). In clinical settings, the acquisition of these heavily T2-weighted MR images of good quality

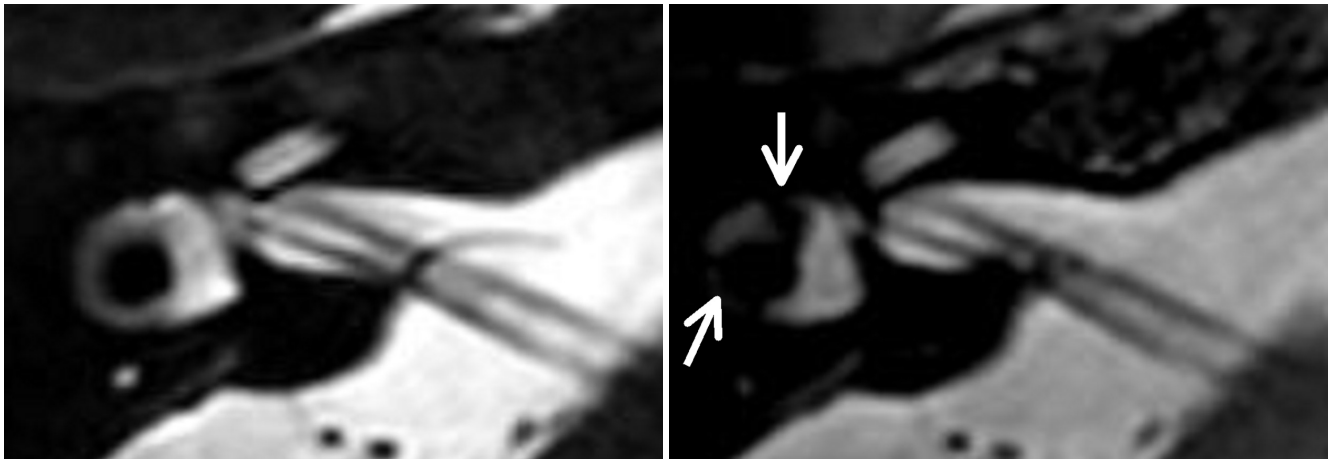

A **B**

Fig. 2. Comparison of 3D driven equilibrium and 3D balanced fast field echo sequences for visualization of vestibule and lateral semicircular canal. While vestibule and lateral semicircular canal are clearly seen without any areas of signal loss on 3D driven equilibrium image (**A**), there are significant blackouts (arrows) due to susceptibility artifacts as seen on 3D balanced fast field echo image (**B**).

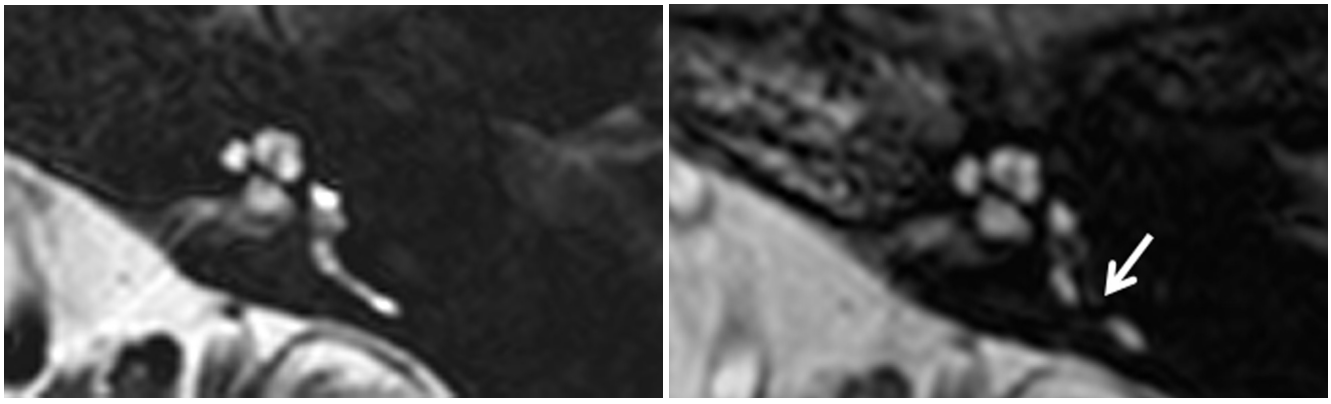

A **B**

Fig. 3. Comparison of 3D driven equilibrium and 3D balanced fast field echo sequences for visualization of posterior semicircular canal. While entire posterior semicircular canal is well seen on 3D driven equilibrium image (**A**), there is large area of signal loss (arrow) on 3D balanced fast field echo image (**B**).

requires not only a high signal from the fluid-containing spaces and less of artifacts from motion and magnetic susceptibility, but also a short examination time (6, 8, 9, 13).

Although those FSE- and FGRE-based 3D MR imaging techniques provide high spatial-resolution MR imaging of the temporal bone with a consistent cisternographic effect, both have inherent disadvantages that cannot be ignored. The major drawback of 3D FGRE techniques is a high sensitivity to magnetic susceptibility. Although multiple refocusing pulses and short echo spacing produce less susceptibility artifacts with 3D FSE techniques, a relatively long scan time and inconsistent cisternographic effect despite gradient moment nulling are the major drawbacks (14). Two methods currently used for compensating for these inherent drawbacks of 3D FSE techniques include shortening of the TR and an increase of the echo train length. The major trade-offs are a reduced cisternographic effect due to an increased T1 effect for the former and image blurring from T2-decay-induced modulations in the amplitude of the echo in the k space for the latter (14, 16). Several modifications of 3D T2-weighted FSE and FGRE MR imaging techniques have been developed to improve the shortcomings inherent to each sequence without the loss of image quality.

In this study, we compared the use of 3D DRIVE and 3D bFFE sequences, both of which are considered currently as state-of-the-art imaging methods for MR cisternography. DRIVE, also called FRFSE, is an FSE sequence that uses a set of additional -90° recovery pulses applied at the end of the echo train to revert the remaining transverse magnetization back to the longitudinal axis. These reset pulses allow heavily T2-weighted images to be acquired with a shorter TR and reduce the scan time considerably (5, 9, 12–14). The shortened TR also has the effect of reducing flow void artifacts, further increasing the brightness of fluids. In contrast, bFFE is an FGRE sequence that utilizes a very short TR and radiofrequency pulses with a large flip angle. A balanced gradient waveform is used for all gradient directions to provide a very high signal for tissues with a high T2/T1 ratio. Complete balancing of the gradients is achieved by repeated application of equidistant radiofrequency pulses (8, 10, 13). bFFE is rather resistant to motion and flow as phase shifts within the imaging plane are refocused (13). The maximum intrinsic flow compensation is achieved when the TE is half of the TR. However, as with the other GRE techniques, bFFE is still sensitive to magnetic field inhomogeneities represented by zebra stripe artifacts seen in the images. The severity of the artifacts is roughly proportional to field strength and TR.

In the present study, 3D DRIVE was generally better than 3D bFFE for the evaluation of the cranial nerves within the IAC and the fine anatomic structures of the inner ear. As for demonstration of the inner ear structures, our results are concordant with those of Naganawa et al. (6) and Jung et al. (13), who reported that 3D FSE sequences using FASE and DRIVE were superior to 3D FGRE sequences using CISS and bFFE, respectively. These investigators postulated that the poor image quality of CISS and bFFE would result from the banding artifact induced by the strong magnetic susceptibility effect inherent to the GRE techniques. This banding artifact can simulate labyrinthine pathology and is more problematic at 3T than at 1.5T, because susceptibility changes linearly with field strength (12). As for demonstration of the cranial nerves within the IAC, however, our results are discordant with those of Tsuchiya et al. (10), who reported that 3D bFFE was somewhat superior to 3D FRFSE due to the higher CNRs and less CSF pulsation artifacts. In the present study, however, CSF pulsation artifacts did not hamper the evaluation of the cranial nerves in the CPA cistern and IAC as determined by the 3D DRIVE sequence as well as the 3D bFFE sequence. The lack of significant CSF pulsation artifacts with the 3D DRIVE sequence might be partly attributed to the reduced echo train length of 40 used in this study instead of 74 used in the previous study, and also to usage of an 8-channel SENSE head coil with a SENSE factor of 2 (a factor of 2 is associated with a 40% reduction in the signal-to-noise ratio [SNR] and a 50% reduction in imaging time) that made it possible to obtain MR images of improved quality without lengthening the acquisition time. Our results are also discordant with those of Lane et al. (12). In a study with a 3T MR scanner on imaging of the cochlear nerve and labyrinth, Lane and colleagues (12) preferred the use of 3D CISS to 3D FRFSE, because of the superior CNRs seen in the former sequence. There is no clear answer to explain the different results obtained in the two studies. Although we did not perform quantitative analysis, the combination of several factors such as the differences between quantitative and qualitative analyses, errors obtained during measurements of CNRs, the use of parallel imaging, and the technical differences between various 3D FSE and FGRE sequences according to different vendors could all be factors that contributed to the results obtained.

The imaging time of MR examinations is dependent on the TR, matrix size, and NSA. With the same matrix size of 336×335, we used one NSA for 3D DRIVE and five NSAs for 3D bFFE in this study. The acquisition times for 3D DRIVE and 3D bFFE were 5 minutes 26 seconds and 3 minutes 59 seconds, respectively, with no significant patient motion artifact. In this study, without application of

a SENSE factor of 2, the acquisition time of DRIVE imaging would be expected to double, which seems to be rather unacceptable in a clinical setting.

The most renowned advantage of the use of 3T over 1.5T is the increased SNR of the higher field strength. Theoretically, a doubling of signal to noise is expected from 1.5 to 3.0T, as magnetization increases as the square of the field strength, while noise increases linearly. However, the actual increase of SNR at 3T has been reported on the order of 30–60% (17). Another important issue is the characteristics of current 3T devices that are inherently more SAR efficient. Because SAR scales with the square of the field strength, radiofrequency deposition is more limiting at MR with higher field strengths (18). The SAR can be a more problem with 3D FGRE imaging than with 3D FSE imaging. In a study with 1.5T, Naganawa et al. (6) reported that the mean SAR was higher with the 3D FGRE sequence than with the 3D FSE sequence (0.053 W/kg for 3D CISS versus 0.019 W/kg for 3D FASE). In our study, both 3D DRIVE and 3D bFFE sequences using an 8-channel SENSE head coil satisfied the SAR limitation at 3T. As could be expected, our study showed greatly increased SAR values, compared to the previous study that used 1.5T. Our study also showed that the mean SAR was significantly higher with the 3D FGRE sequence than with the 3D FSE sequence (2.3 W/kg for 3D bFFE versus 0.9 W/kg for 3D DRIVE).

In this study, we did not perform quantitative analysis to compare the CNRs of the cranial nerves between the use of 3D DRIVE and 3D bFFE. This was because a direct reliable measurement of background noise was mostly impossible with a SENSE technique that can induce artificial suppression of background noise (13, 15). Although it was not employed in this study, an alternative method for measurement of CNR with a SENSE technique is to calculate the relative contrast. Instead of calculating CNRs by direct measurement of background noise, the relative contrast is calculated by referring the cranial nerve signal intensity to that of CSF. In a study with SENSE at 1.5T, Jung et al. (13) reported that the DRIVE sequence provided images that had higher relative contrast for the facial nerve and cerebellum than the 3D bFFE sequence. Likewise, in a study without SENSE at 1.5T (10), the relative contrast of the 3D bFFE sequence was inferior to that of the 3D FRFSE sequence, although the CNR of the 3D bFFE sequence was better.

In conclusion, both 3D DRIVE and 3D bFFE sequences at 3T with the SENSE technique can provide heavily T2-weighted MR images of reasonable quality for the evaluation of the cranial nerves within the IAC and fine anatomic structures of the inner ear. However, because of a higher image quality and less susceptibility artifacts, we highly recommend the use of 3D DRIVE imaging as the MR imaging choice for the IAC and inner ear.

References

1. Casselman JW, Kuhweide R, Deimling M, Ampe W, Dehaene I, Meeus L. Constructive interference in steady state-3DFT MR imaging of the inner ear and cerebellopontine angle. *AJNR Am J Neuroradiol* 1993;14:47-57
2. Held P, Fellner C, Fellner F, Seitz L, Graf S, Hilbert M, et al. MRI of inner ear and facial nerve pathology using 3D MP-RAGE and 3D CISS sequences. *Br J Radiol* 1997;70:558-566
3. Naganawa S, Ito T, Fukatsu H, Ishigaki T, Nakashima T, Ichinose N, et al. MR imaging of the inner ear: comparison of a three-dimensional fast spin-echo sequence with use of a dedicated quadrature-surface coil with a gadolinium-enhanced spoiled gradient-recalled sequence. *Radiology* 1998;208:679-685
4. Yang D, Kodama T, Tamura S, Watanabe K. Evaluation of the inner ear by 3D fast asymmetric spin echo (FASE) MR imaging: phantom and volunteer studies. *Magn Reson Imaging* 1999;17:171-182
5. Schmalbrock P. Comparison of three-dimensional fast spin echo and gradient echo sequences for high-resolution temporal bone imaging. *J Magn Reson Imaging* 2000;12:814-825
6. Naganawa S, Koshikawa T, Fukatsu H, Ishigaki T, Fukuta T. MR cisternography of the cerebellopontine angle: comparison of three-dimensional fast asymmetrical spin-echo and three-dimensional constructive interference in the steady-state sequences. *AJNR Am J Neuroradiol* 2001;22:1179-1185
7. Nakashima K, Morikawa M, Ishimaru H, Ochi M, Kabasawa H, Hayashi K. Three-dimensional fast recovery fast spin-echo imaging of the inner ear and the vestibulocochlear nerve. *Eur Radiol* 2002;12:2776-2780
8. Nakamura T, Naganawa S, Koshikawa T, Fukatsu H, Sakurai Y, Aoki I, et al. High-spatial-resolution MR cisternography of the cerebellopontine angle in 90 seconds with a zero-fill interpolated fast recovery 3D fast asymmetric spin-echo sequence. *AJNR Am J Neuroradiol* 2002;23:1407-1412
9. Ciftci E, Anik Y, Arslan A, Akansel G, Sarisoy T, Demirci A. Driven equilibrium (drive) MR imaging of the cranial nerves V-VIII: comparison with the T2-weighted 3D TSE sequence. *Eur J Radiol* 2004;51:234-240
10. Tsuchiya K, Aoki C, Hachiya J. Evaluation of MR cisternography of the cerebellopontine angle using a balanced fast-field-echo sequence: preliminary findings. *Eur Radiol* 2004;14:239-242
11. Naganawa S, Koshikawa T, Fukatsu H, Ishigaki T, Aoki I, Ninomiya A. Fast recovery 3D fast spin-echo MR imaging of the inner ear at 3T. *AJNR Am J Neuroradiol* 2002;23:299-302
12. Lane JI, Ward H, Witte RJ, Bernstein MA, Driscoll CL. 3-T imaging of the cochlear nerve and labyrinth in cochlear-implant candidates: 3D fast recovery fast spin-echo versus 3D constructive interference in the steady state techniques. *AJNR Am J Neuroradiol* 2004;25:618-622
13. Jung NY, Moon WJ, Lee MH, Chung EC. Magnetic resonance cisternography: comparison between 3-dimensional driven equilibrium with sensitivity encoding and 3-dimensional balanced fast-field echo sequences with sensitivity encoding. *J Comput Assist Tomogr* 2007;31:588-591

14. Melhem ER, Itoh R, Folkers PJ. Cervical spine: three-dimensional fast spin-echo MR imaging—improved recovery of longitudinal magnetization with driven equilibrium pulse. *Radiology* 2001;218:283-288
15. Preibisch C, Pilatus U, Bunke J, Hoogenraad F, Zanella F, Lanfermann H. Functional MRI using sensitivity-encoded echo planar imaging (SENSE-EPI). *Neuroimage* 2003;19:412-421
16. Constable RT, Gore JC. The loss of small objects in variable TE imaging: implications for FSE, RARE, and EPI. *Magn Reson Med* 1992;28:9-24
17. Ross JS. The high-field-strength curmudgeon. *AJNR Am J Neuroradiol* 2004;25:168-169
18. Tanenbaum LN. 3-T MR imaging: ready for clinical practice. *AJNR Am J Neuroradiol* 2004;25:1626-1627